Atmos. Chem. Phys. Discuss., 11, 22173–22198, 2011
www.atmos-chem-phys-discuss.net/11/22173/2011/
doi:10.5194/acpd-11-22173-2011

Atmospheric Chemistry and Physics Discussions

Stratospheric ozone chemistry in the Antarctic: what controls the lowest values that can be reached and their recovery?

J.-U. Grooß[1], K. Brautzsch[1], R. Pommrich[1,2,3], S. Solomon[4], and R. Müller[1]

[1]Institut für Energie- und Klimaforschung – Stratosphäre (IEK-7), Forschungszentrum Jülich, Germany
[2]Laboratoire d'Aérologie, CNRS/INSU-Université de Toulouse, Toulouse, France
[3]Groupe d'étude de l'Atmosphère Météorologique, CNRM-GAME, Météo-France, Toulouse, France
[4]Department of Atmospheric and Oceanic Science, University of Colorado, Boulder, CO, USA

Received: 27 July 2011 – Accepted: 2 August 2011 – Published: 5 August 2011

Correspondence to: J.-U. Grooß (j.-u.grooss@fz-juelich.de)

Published by Copernicus Publications on behalf of the European Geosciences Union.

Abstract

Balloon-borne observations of ozone from Antarctic stations have been reported to reach ozone mixing ratios as low as about 10 ppbv at the 70 hPa level by late September. After reaching a minimum, ozone mixing ratios then increase to the ppmv level by late December. While the basic mechanisms causing the ozone hole have been known for more than 20 yr, the detailed chemical processes controlling how low the local concentration can fall, and how it recovers from the minimum have not been explored so far. Both of these aspects are investigated here by analysing results from the Chemical Lagrangian Model of the Stratosphere (CLaMS). We discuss the processes responsible for stopping of the catalytic ozone depletion. We show that an irreversible chlorine deactivation into HCl can occur either when ozone drops to very low values or by temperatures increasing above the PSC threshold in these simulations. As a consequence, the timing and mixing ratio of the minimum depends sensitively on model parameters including the ozone initialisation. The subsequent observed ozone increase between October and December is linked not only to transport, but also to photochemical ozone production, caused by oxygen photolysis and by the oxidation of carbon monoxide and methane.

1 Introduction

Since the discovery of the ozone hole (Farman et al., 1985), the chemical mechanisms causing ozone depletion have been clarified (e.g., Solomon, 1999; WMO, 2011). These mechanisms yield an almost complete destruction of ozone in certain altitudes in the Antarctic stratosphere as observed in observations of ozone sondes over four decades (Solomon et al., 2005). Figure 1 shows the ozone observations from South Pole station at the 70 hPa level. The logarithmic ordinate highlights the massive loss of ozone at these altitudes, with ozone mixing ratios falling to and below the approximate instrument detection limit of 10 ppbv (see Vömel and Diaz, 2010) by late September

ACPD
11, 22173–22198, 2011

and early October above the South Pole station. When ozone is plotted on a logarithmic scale against time of year, the key role of transport of air not depleted in ozone over the station is evident; thus a few observations display high ozone abundances similar to the pre-ozone hole values. However, the graph also reveals a lower envelope of the observations that is nearly the same in different years since 1990, characterising the chemical decay of ozone to values as low as 10 ppbv around the end of September and increasing again afterwards. While the basic mechanisms for the rapid ozone loss are understood, the explanation for the ozone depletion to be limited to values near 10 ppbv have not yet been explained, nor has the factor driving the subsequent increase been identified. Here we use simulations of the Chemical Lagrangian Model of the Stratosphere (CLaMS) to investigate these processes.

2 Model description

The simulations presented here are performed with the Chemical Lagrangian Model of the Stratosphere (McKenna et al., 2002a,b; Konopka et al., 2004; Grooß et al., 2005b). Here the model is used in two different modes. In the box model mode, stratospheric chemistry is calculated for a few example air parcels along their trajectory whereas the global mode is the Lagrangian 3-dimensional Chemistry Transport Model.

In the box-model mode, the air parcels are defined here by a location and time of ozone soundings in the ozone hole period, from which trajectories are calculated both backward to June and forward to December. Simulations with the CLaMS chemistry module are then performed forward in time using the combination of these two trajectories. The trajectories of the air parcels were calculated using wind and temperature data from the ECMWF operational analysis. CLaMS includes options for different solvers to integrate the system of stiff ordinary differential equations resulting from the chemistry (Carver et al., 1997; McKenna et al., 2002b). The photolysis rates are calculated in spherical geometry (Meier et al., 1982; Becker et al., 2000) using a climatological ozone profile for ozone hole conditions from HALOE (Grooß and Rus-

ACPD
11, 22173–22198, 2011

sell, 2005). Heterogeneous chemistry is calculated on ice, nitric acid trihydrate (NAT), and liquid ternary $H_2O/H_2SO_4/HNO_3$ particles. The parameterisations of the uptake coefficient to model heterogeneous chemistry on liquid aerosols are derived from Hanson (1998) and those on NAT particles are derived from Hanson and Ravishankara (1993). NAT formation is assumed to occur at a HNO_3 supersaturation of a factor of 10, corresponding approximately to 3 K supercooling below T_{NAT}.

In the box-model mode, we use the solver SVODE (Brown et al., 1989) that does not use the family approximation which could become invalid at very low ozone mixing ratios. Also, no denitrification parameterisation was used in the box-model mode, therefore chemical consequences of the denitrification were addressed by sensitivity studies. The chemical initialisation for the air-parcels in the box-model mode is interpolated from the 3-dimensional CLaMS simulations described below. The results from such box model studies do not include mixing between neighbouring air masses nor denitrification due to sedimentation of HNO_3-containing particles. Over this long time span, a trajectory should not be viewed as representing the exact location of a single airmass. Rather it should be interpreted as one of the possible approximate histories of an air parcel that reaches low mixing ratios. Thus, the results of this trajectory-box model can be used to investigate the chemical processes around the observed minimum ozone mixing ratios.

The CLaMS 3-D simulations for the ozone hole in the year 2003 were described in detail in a diploma thesis (Walter, 2005), and are continued until the end of December in this work. They were initialised on 1 May 2003 using observations from various sources (MIPAS, ILAS-II), including tracer correlations for Cl_y, Br_y (Grooß et al., 2002), and NO_y (Grooß et al., 2005a). The remaining species were initialised from a 2-D model (Grooß, 1996). Denitrification by sedimenting NAT particles was simulated with the scheme that was used for the Arctic winter 2002/2003 (Grooß et al., 2005a). The horizontal resolution of this simulation is 100 km between 40 and 90° S. Here, the solver IMPACT was used that is based on the family concept approximation (Carver and Scott, 2000).

ACPD
11, 22173–22198, 2011

3 Results

For determining the chemical processes around the ozone minimum in late September, a trajectory was chosen such that it exactly intersects an observation from the South pole station of about 10 ppbv ozone in the pressure level of 70 hPa on 24 September 2003. The box-model simulation was performed for this trajectory with the time period from 1 June to 30 November 2003. This trajectory should be taken as an example of the possible development for which the chemistry is investigated in detail. Figure 2 shows the development of the relevant chemical species and rates in the single box of the simulation. Panel a shows the potential temperature of the air parcel with the typical diabatic descent in the polar vortex and panel b shows the temperature along the trajectory. In panel c we show simulated ozone mixing ratio. The chosen sonde observation that determined the trajectory is plotted as a black star symbol. It is clear that the simulation does reach ozone mixing ratios as low as those observed by the sondes.

3.1 Chlorine deactivation and heterogeneous chemistry

We first focus on the time period of two weeks before the simulated ozone minimum (grey shaded area in Fig. 2). The simulation shows that the cessation of ozone loss (yielding a minimum near 10 ppbv) depends upon a very fast deactivation of active chlorine compounds into the reservoir species HCl only on the time scale of about a day. Although the temperatures are still low enough for NAT existence, thus chlorine activation on liquid and solid particles would be still possible, chlorine activation does not occur after the ozone minimum, because practically all inorganic chlorine is in the form of HCl, and neither $ClONO_2$ nor HOCl are available as a reaction partner for HCl in one of the heterogeneous chlorine activation reactions. Figure 3 shows the pathways of chlorine activation and chlorine deactivation in a simplified way. The main chlorine activation reaction is $ClONO_2$+HCl from which after Cl_2 photolysis ClO_x is produced. The deactivation reactions Cl+CH_4 and ClO+NO_2 then re-form the chlorine

ACPD
11, 22173–22198, 2011

reservoirs $ClONO_2$ and HCl, respectively. This chain stops if all chlorine compounds are deactivated into HCl.

In the example shown in Fig. 2, the chlorine deactivation into the reservoir HCl occurs in the short time period of only about one day. Figure 2f shows the net chlorine activation and deactivation rates. The blue line corresponds to the sum of all reactions that decompose HCl or $ClONO_2$, mainly the heterogeneous reactions of $ClONO_2$+HCl, $ClONO_2$+H_2O and HOCl+HCl. The red line corresponds to the sum of all reactions in which $ClONO_2$ or HCl are formed, mainly ClO+NO_2, Cl+CH_4, and Cl+CH_3OOH. It is visible that these rates are approximately balanced and they increase to values of the order of 10 ppbv per day in the period before the ozone minimum. The deactivation rate would lead to a complete chlorine deactivation within about 6 h if heterogeneous chlorine activation were not occurring at the same time.

For a better focus on the short time period before the minimum ozone occurs, Fig. 4 shows the model results for this two week period again, but as a function of ozone mixing ratio on a logarithmic scale. The time is indicated by the grey shadings that correspond to every second day while lower ozone mixing ratios correspond to the later times of the period. Panel a of this figure shows the temperature and panel b shows how the development of chlorine species depends on ozone for the chosen example. It is evident that below 0.1 ppmv ozone, HCl increases rapidly until no other chlorine compounds than HCl are present in significant amounts. At this point, the ozone minimum is reached. Panel c of Fig. 4 shows the simulated rates for chlorine activation and deactivation. As long as it is cold enough for the presence of PSCs and as long as the formation of $ClONO_2$ by the reaction ClO + NO_2 is occurring, the chlorine deactivation is immediately followed by heterogeneous chlorine activation through the reaction HCl+$ClONO_2$. In the case of temperatures near or above 195 K (e.g. in Fig. 4 at 0.7 ppmv of ozone), the chlorine activation rate sinks below the deactivation rate. With decreasing ozone mixing ratios, the chlorine deactivation rate into HCl increases such that HCl is formed, in the indicated example between 0.02 and 0.004 ppmv despite the low temperatures. The role of ozone in controlling the re-formation of chlorine

ACPD
11, 22173–22198, 2011

reservoirs HCl and $ClONO_2$ in polar spring was first noted by Douglass et al. (1995). For low ozone mixing ratios the formation of HCl is strongly dominant. The main reason for the increase in chlorine deactivation rate with decreasing ozone mixing ratio is the strongly increasing Cl/ClO ratio (Douglass et al., 1995; Grooß et al., 1997) that is plotted in panel d. Due to this dependency, the net chlorine deactivation rate into HCl increases with decreasing ozone mixing ratio. The ozone mixing ratio is low enough that the formation of HCl dominates over chlorine activation as ozone drops below about 0.1 ppmv. The positive feedback between decrease in ozone and increase in chlorine deactivation rate leads to chlorine being irreversibly de-activated. In other words, the low ozone mixing ratios drive the chlorine deactivation. The specific ozone mixing ratio at which this complete chlorine deactivation happens, depends critically on the composition and temperature history of the air parcel, as will be shown below. From Fig. 4 it can also be seen that during darkness no major changes of the chemical composition occur. The active chlorine ClO_x is then predominantly in the form of Cl_2O_2 that does not photolyse. Thus, no ozone depletion or significant change in chlorine activation occurs during darkness.

We also investigated the catalytic cycles responsible for the ozone depletion and their behaviour in this 14-day period. The rate limiting steps of the most important catalytic destruction cycles are plotted in Fig. 2g and e. The most effective catalytic ozone loss cycles are the ClO-dimer cycle (Molina and Molina, 1987) and the ClO-BrO cycle (McElroy et al., 1986) plotted in orange and green, respectively. Other catalytic ozone loss cycles of which only the BrO-BrO cycle is shown are much less effective.

After the ozone minimum is reached, the sum of the ozone loss rates falls below the ozone production (black dotted lines) caused by oxygen photolysis (black solid line) and other ozone production chains that are discussed below.

3.2 Sensitivity studies

In this section we investigate the sensitivity of the simulated ozone mixing ratio with respect to several model assumptions. For that purpose, we first performed additional

ACPD
11, 22173–22198, 2011

box model simulations identical to the one described above but with a slightly different initial ozone mixing ratio. Figure 5 shows four additional simulations in which the initial ozone mixing ratio was changed between 2.6 and 3.2 ppmv. Surprisingly, each of the four simulations shows both, very different minimum ozone mixing ratio and different times when this minimum is reached. Moreover, there is no obvious relationship between the initial ozone mixing ratio and either the time or the minimum ozone mixing ratio. A similar comparison for a trajectory through a different ozone-sonde observation also shows this behaviour (not shown). The reason for this behaviour of the model results was investigated by looking at the differences to the reference simulation. Similar to the reference simulation, in the sensitivity runs the ozone depletion was terminated by an irreversible chlorine de-activation into HCl, after which no chlorine activation occurred despite PSC surfaces being available. The chlorine de-activation can occur when temperatures temporarily rise above around 195 K, i.e. above the threshold temperature for chlorine activation. As explained above, also the formation of HCl is increasingly favoured with decreasing ozone mixing ratio. Even though the individual air parcel trajectory is identical in all of the simulations shown in Fig. 5, the low ozone mixing ratios below about 0.1 ppmv are reached at a different time and thus at a different temperature. It is therefore possible that in two almost equal simulations with only a slightly different ozone initialisation, one simulation shows complete irreversible chlorine de-activation into HCl at a relatively large ozone mixing ratio, while in other simulations some active chlorine could remain giving the possibility of $ClONO_2$ formation, later chlorine activation and further ozone depletion. The lowest ozone mixing ratios were reached when the temperature at the ozone minimum stayed below 190 K the last days before the ozone minimum. The sensitive dependence of the timing of the deactivation on temperature and low ozone mixing ratios makes it nearly impossible to simulate the exact ozone minimum for a single air parcel at least in some cases. It gives also a possible explanation for the variability of ozone observations reported by Solomon et al. (2005).

ACPD
11, 22173–22198, 2011

The simulated ozone mixing ratios also depend on other prerequisites as the initial chlorine activation. This was investigated by repeating the above simulations but initialised with a larger initial chlorine activation in which about 75 % instead of 50 % of Cl_y was initialised as ClO_x. One result of the increased chlorine activation is of course faster ozone depletion at the beginning of the spring season. However, the general behaviour of the temporal development of simulated ozone dependence on the initial ozone mixing ratio remained (not shown).

The vertical re-distribution of NO_y due to sedimenting HNO_3-containing particles is only considered in the 3-dimensional CLaMS simulation. However, in the box model simulation it is possible to include denitrification by removing HNO_3 from the model when NAT is present by a simple parametrisation (Grooß et al., 2002). This parametrisation was used here to study the sensitivity with respect to denitrification. The denitrification was adjusted such that about 3 ppbv of HNO_3 remained in the box in November, consistent with ACE-FTS observations (Jones et al., 2011). Individual simulations look different when the denitrification is included and all other model parameters remain identical. Due to less available NO_2, the formation of $ClONO_2$ is slower and also less HNO_3 causes lower surfaces of solid and liquid PSCs. With the denitrification parametrisation, the maximum of the chlorine deactivation rate is about 50 % lower than for the reference simulation. However, also here the general behaviour of the temporal development of simulated ozone dependence on the initial ozone mixing ratio remained (not shown). Denitrification also causes a slower increase in the rate in ozone after the minimum as will be discussed below.

3.3 Ozone recovery

From the observations shown in Fig. 1, it is evident that after early October the lower envelope of the ozone observations increases again with time. Possible explanations for this increase could be either in-situ production of ozone or mixing with air masses containing larger ozone mixing ratios. However, the increase occurs smoothly, suggesting a likely role for chemistry rather than dynamics alone, which would be expected to

ACPD
11, 22173–22198, 2011

be episodic and variable. In the box model results, the in-situ ozone production can be probed. To investigate the latitude and altitude dependence of the in-situ ozone production, multiple box model simulations have been performed on artificial trajectories in which latitude, temperature and pressure level have been kept constant over the period of October through December.

These simulations were initialised without chlorine activation ($HCl = Cl_y$), 1 ppbv ozone, and 4.5 ppbv NO_y corresponding to moderate denitrification. The analysis of these simulations shows that three reaction chains are responsible for the ozone production. One of these is the well known production by oxygen photolysis (Chapman, 1930).

$$\begin{aligned} \mathbf{O_2 + h\nu} &\rightarrow \mathbf{2O} \\ O + O_2 + M &\rightarrow O_3 \quad (2\times) \\ \hline 3O_2 &\rightarrow 2O_3 \end{aligned} \tag{1}$$

Two other reaction chains make important contributions to the modeled ozone production, the oxidation of CO and CH_4.

$$\begin{aligned} \mathbf{CO + OH} &\rightarrow \mathbf{H + CO_2} \\ H + O_2 + M &\rightarrow HO_2 \\ HO_2 + NO &\rightarrow NO_2 + OH \\ NO_2 + h\nu &\rightarrow NO + O \\ O + O_2 + M &\rightarrow O_3 \\ \hline CO + 2O_2 &\rightarrow CO_2 + O_3 \end{aligned} \tag{2}$$

and

ACPD
11, 22173–22198, 2011

$$\mathbf{CH_4 + Cl \rightarrow CH_3 + HCl}$$
$$\mathrm{HCl + OH \rightarrow Cl + H_2O}$$
$$\mathrm{CH_3 + O_2 + M \rightarrow CH_3OO}$$
$$\mathrm{CH_3OO + NO \rightarrow NO_2 + CH_2O + H}$$
$$\mathrm{H + O_2 + M \rightarrow HO_2}$$
$$\mathrm{HO_2 + NO \rightarrow NO_2 + OH}$$
$$\mathrm{NO_2 + } h\nu \mathrm{ \rightarrow NO + O} \quad (2\times)$$
$$\mathrm{O + O_2 + M \rightarrow O_3} \quad (2\times)$$

$$\mathrm{CH_4 + 4O_2 \rightarrow CH_2O + H_2O + 2O_3} \quad (3)$$

Alternatively the first 2 reactions of reaction chain (Eq. 3) replaced by the following reaction resulting in a chain with the same sum reaction.

$$\mathbf{CH_4 + OH \rightarrow CH_3 + H_2O} \quad (4)$$

A further minor ozone production chain is also initiated by the oxidation of CH_2O that is not elaborated here. In each of the above reaction chains, the slowest reaction that determines the ozone production rate is written in bold face. (Note that in the presence PSCs and active chlorine, the heterogeneous reaction $ClONO_2 + HCl$ occurs parallel to $HCl + OH$ in reaction chain (3). In that case rather the reaction $CH_3OO + NO$ determines the rate of cycles 3 and 4.) The simulations showed that the ozone production rates of reactions cycles (2 to 4) are of the order of 1 ppbv per day and therefore relatively unimportant for typical stratospheric ozone mixing ratios. These cycles are only of importance here due to the low solar elevation. Figure 6 shows the simulated ozone increase between 1 October and 30 November for three pressure levels 100, 70, and 50 hPa. The dashed line corresponds to the ozone increase due to oxygen photolysis only (cycle 1). The dotted lines correspond to the sum of the rate-limiting

ACPD
11, 22173–22198, 2011

rates of reaction chains (1) to (4) including oxygen photolysis. It is slightly larger than the calculated net ozone production (solid lines), because also some ozone depletion cycles are occurring (see also Fig. 2g).

In Figs. 2g and 4e the dotted black lines correspond to the ozone production rate due to the sum of all ozone production chains (1) to (4). This part of the ozone production increases with increasing altitude. It increases also with distance to the south pole due to the higher solar elevation. The part of ozone production caused by the CH_4 oxidation (cycles 2 and 3) corresponds to the difference between the dotted and the dashed line. It stays approximately constant with altitude and latitude.

For the results shown in Fig. 6, the oxygen photolysis rate was calculated using a climatological overhead ozone profile (Grooß and Russell, 2005) that contains average ozone mixing ratios for the ozone hole time period. However, it is possible that the ozone profile above the observations with very low ozone mixing ratio at the lower envelope may also be significantly below average. This would cause an increase in the oxygen photolysis rate and therefore in the ozone production rate. To investigate this sensitivity, we repeated the simulations assuming a reduced overhead ozone profile. It was reduced by a factor of 5 between 30 and 150 hPa south of 65° S. The results with this reduced overhead ozone profile are displayed in Fig. 7. A larger ozone production is evident, especially at the 50 hPa level towards the vortex edge. However, air masses with ozone mixing ratios well below average may not remain vertically aligned over the period of two months.

The ozone production rate due to cycles (2) and (3) depends on the available nitrogen compounds and is strongly influenced by the denitrification. A decrease in NO_y implies also a decrease in NO_x (=NO + NO_2). The NO_x-dependence of ozone production rates was already investigated in the context evaluating of aircraft emissions (e.g. Grooß et al., 1998). Figure 8 shows the sensitivity with respect to NO_y between 2.5 and 8 ppbv for the simulation at the 70 hPa level. Figure 8 shows that the in-situ ozone increase is slower for more denitrified air. This demonstrates the importance of production due to CO and CH_4 oxidation. An increase in NO_x increases the Cl/ClO ratio

ACPD
11, 22173–22198, 2011

due to the faster reaction NO + ClO and the OH/HO_2 ratio due to the faster reaction NO + HO_2.

For comparison with the range of observed ozone observations, we show now box model simulations for realistic trajectories that include diabatic descent and latitude variations. The box model simulations of the same kind as shown in Sect. 3.1 were initialised on 1 August interpolated from the 3-dimensional CLaMS CTM simulation. The vertical coordinate for that comparison is potential temperature instead of pressure that was used in Fig. 1. To first order, potential temperature is conserved within air parcels, such that a comparison with the box model results is more appropriate on potential temperature levels. There is some diabatic descent for the indicated trajectories, but it is below 10 K for the lower three levels (375 K, 400 K, 450 K) and 19 ± 5 K for the 500 K level for the period between the time at the South pole and 1 December. Part of the ozone increase in November and December on the 70 hPa level (Fig. 1) is neither photochemical ozone production nor mixing. It is caused by the fact that due to the annual cycle of the temperatures, data on different potential temperature levels are compared over the course of the season in Fig. 1. The change in potential temperature at 70 hPa between 1 October and 1 December is about 38 K.

Here, the box model was run for trajectories that pass exactly over the South pole on 21 days (20 September to 10 October 2003) for each of the potential temperature levels 375 K, 400 K, 450 K, and 500 K. Although the latitude of trajectories changes with time, we argue that the simulated chemical ozone production should be similar to the South pole observations, because, to first order, similar ozone loss would be expected for an air parcel starting at the pole and ending at latitude *x* compared with an air parcel starting at latitude *x* and ending at the pole for the same time period. Also the results of single box model runs can only be taken as an example, since the development of the results very sensitively depend on the initial ozone mixing ratio as shown in the previous sections. The simulated ozone mixing ratios for these simulations are shown in Fig. 9. Generally it can be seen that the simulations overlay the area of observations. In the 375 K and 400 K levels, the simulated ozone for many example trajectories follow

ACPD
11, 22173–22198, 2011

the lower envelope of the ozone observations well. On the 500 K potential temperature level, the majority of the box-model simulations have ozone mixing ratios below the lower envelope of the observations. Part of this difference may be resolved if diabatic descent were taken into account. Generally, mixing of air masses which is not considered in the box model simulations would also yield an increase in ozone.

The CLaMS-3D simulation fails to reach the minimum ozone mixing ratios that are seen in the observations, probably due to the low resolution of the model simulation. However, one can see especially on the 400 K and 450 K level that the increase in ozone in October and November is faster than that in the box model simulations. This additional increase might be explained by the mixing, as represented and potentially over-estimated in the 3-D CLaMS simulation. But from the shown results it is clear that in-situ ozone productions by the reaction chains mentioned above can explain much of the observed ozone increase in October and November.

4 Conclusions

In this paper, we have eludicated several processes that are responsible for Antarctic ozone depletion. We showed that the observed very low ozone mixing ratios can be reproduced in box model simulations. A critical constraint on the minimum ozone that can be reached is fast irreversible chlorine de-activation into HCl, which is triggered by very low ozone mixing ratios and makes the ozone loss self-limiting. Ozone depletion can end even though surfaces of solid or liquid PSC particles are still available for heterogeneous reactions. The timing and the value of this minimum ozone mixing ratio is very sensitive to different model parameters, in particular the initial ozone mixing ratio, therefore it is not possible in all cases to exactly predict these parameters for a single air mass. The increase of the ozone mixing ratios after the minimum is be mostly explained by in-situ chemical ozone production both by oxygen photolysis and as a consequence of methane and carbon monoxide oxidation. Additional ozone increase caused by mixing is also possible, particularly for later times in the spring season.

ACPD
11, 22173–22198, 2011

Acknowledgements. We thank Herman Smit and Peter von der Gathen for helpful discussions on the detection limit of ozone sondes.

References

Becker, G., Grooß, J.-U., McKenna, D. S., and Müller, R.: Stratospheric photolysis frequencies: Impact of an improved numerical solution of the radiative transfer equation, J. Atmos. Chem., 37, 217–229, doi:10.1023/A:1006468926530, 2000. 22175

Brown, P. N., Byrne, G. D., and Hindmarsh, A. C.: VODE: A variable coefficient ODE solver, SIAM J. Sci. Stat. Comput., 10, 1038–1051, 1989. 22176

Carver, G. D. and Stott, P. A.: IMPACT: an implicit time integration scheme for chemical species and families, Ann. Geophys., 18, 337–346, doi:10.1007/s00585-000-0337-y, 2000. 22176

Carver, G. D., Brown, P. D., and Wild, O.: The ASAD atmospheric chemistry integration package and chemical reaction database, Comput. Phys. Communications, 105, 197–215, 1997. 22175

Chapman, S.: A theory of upper atmospheric ozone, Mem. Roy. Soc., 3, 103–109, 1930. 22182

Douglass, A. R., Schoeberl, M. R., Stolarski, R. S., Waters, J. W., Russell III, J. M., Roche, A. E., and Massie, S. T.: Interhemispheric differences in springtime production of HCl and $ClONO_2$ in the polar vortices, J. Geophys. Res., 100, 13967–13978, 1995. 22179

Farman, J. C., Gardiner, B. G., and Shanklin, J. D.: Large losses of total ozone in Antarctica reveal seasonal ClO_x/NO_x interaction, Nature, 315, 207–210, 1985. 22174

Grooß, J.-U.: Modelling of Stratospheric Chemistry based on HALOE/UARS Satellite Data, PhD thesis, University of Mainz, 1996. 22176

Grooß, J.-U. and Russell III, James M.: Technical note: A stratospheric climatology for O_3, H_2O, CH_4, NO_x, HCl and HF derived from HALOE measurements, Atmos. Chem. Phys., 5, 2797-2807, doi:10.5194/acp-5-2797-2005, 2005. 22175, 22184

Grooß, J.-U., Pierce, R. B., Crutzen, P. J., Grose, W. L., and Russell III, J. M.: Re-formation of chlorine reservoirs in southern hemisphere polar spring, J. Geophys. Res., 102, 13141–13152, doi:10.1029/96JD03505, 1997. 22179

Grooß, J.-U., Brühl, C., and Peter, T.: Impact of aircraft emissions on tropospheric and stratospheric ozone, I: Chemistry and 2-D model results, Atmos. Environ., 32, 3173–3184, 1998. 22184

ACPD

11, 22173–22198, 2011

Grooß, J.-U., Günther, G., Konopka, P., Müller, R., McKenna, D. S., Stroh, F., Vogel, B., Engel, A., Müller, M., Hoppel, K., Bevilacqua, R., Richard, E., Webster, C. R., Elkins, J. W., Hurst, D. F., Romashkin, P. A., and Baumgardner, D. G.: Simulation of ozone depletion in spring 2000 with the Chemical Lagrangian Model of the Stratosphere (CLaMS), J. Geophys. Res., 107, 8295, doi:10.1029/2001JD000456, 2002. 22176, 22181

Grooß, J.-U., Günther, G., Müller, R., Konopka, P., Bausch, S., Schlager, H., Voigt, C., Volk, C.M., and Toon, G. C.: Simulation of denitrification and ozone loss for the Arctic winter 2002/2003, Atmos. Chem. Phys., 5, 1437–1448, doi:10.5194/acp-5-1437-2005, 2005a. 22176

Grooß, J.-U., Konopka, P., and Müller, R.: Ozone chemistry during the 2002 Antarctic vortex split, J. Atmos. Sci., 62, 860–870, 2005b. 22175

Hanson, D. R.: Reaction of $ClONO_2$ with H_2O and HCl in sulfuric acid and $HNO_3/H_2SO_4/H_2O$ mixtures, J. Phys. Chem. A, 102, 4794–4807, 1998. 22176

Hanson, D. R. and Ravishankara, A. R.: Reaction of $ClONO_2$ with HCl on NAT, NAD, and frozen sulfuric acid and hydrolysis of N_2O_5 and $ClONO_2$ on frozen sulfuric acid, J. Geophys. Res., 98, 22931–22936, 1993. 22176

Jones, A., Qin, G., Strong, K., Walker, K. A., McLinden, C., M. Toohey, T., Kerzenmacher, Bernath, P., and Boone, C.: A global inventory of stratospheric NOy from ACE-FTS, J. Geophys. Res., 376, doi:10.1029/2010JD015465, in press, 2011. 22181

Konopka, P., Steinhorst, H.-M., Grooß, J.-U., Günther, G., Müller, R., Elkins, J. W., Jost, H.-J., Richard, E., Schmidt, U., Toon, G., and McKenna, D. S.: Mixing and Ozone Loss in the 1999–2000 Arctic Vortex: Simulations with the 3-dimensional Chemical Lagrangian Model of the Stratosphere (CLaMS), J. Geophys. Res., 109, D02315, doi:10.1029/2003JD003792, 2004. 22175

McElroy, M. B., Salawitch, R. J., Wofsy, S. C., and Logan, J. A.: Antarctic ozone: Reductions due to synergistic interactions of chlorine and bromine, Nature, 321, 759–762, 1986. 22179

McKenna, D. S., Konopka, P., Grooß, J.-U., Günther, G., Müller, R., Spang, R., Offermann, D., and Orsolini, Y.: A new Chemical Lagrangian Model of the Stratosphere (CLaMS): 1. Formulation of advection and mixing, J. Geophys. Res., 107, 4309, doi:10.1029/2000JD000114, 2002a. 22175

McKenna, D. S., Grooß, J.-U., Günther, G., Konopka, P., Müller, R., Carver, G., and Sasano, Y.: A new Chemical Lagrangian Model of the Stratosphere (CLaMS): 2. Formulation of chemistry scheme and initialization, J. Geophys. Res., 107, 4256, doi:10.1029/2000JD000113, 2002b.

ACPD
11, 22173–22198, 2011

22175
Meier, R. R., Anderson, D. E., J., and Nicolet, M.: Radiation Field in the Troposphere and Stratosphere from 240–1000 nm -I: General Analysis, Planet Space Sci., 30, 923–933, 1982. 22175
Molina, L. T. and Molina, M. J.: Production of Cl_2O_2 from the selfreaction of the ClO radical, J. Phys. Chem., 91, 433–436, 1987. 22179
Solomon, S.: Stratospheric ozone depletion: A review of concepts and history, Rev. Geophys., 37, 275–316, doi:10.1029/1999RG900008, 1999. 22174
Solomon, S., Portmann, R. W., Sasaki, T., Hofmann, D. J., and Thompson, D. W. J.: Four decades of ozonesonde measurements over Antarctica, J. Geophys. Res., 110, D21311, doi:10.1029/2005JD005917, 2005. 22174, 22180, 22190
Vömel, H. and Diaz, K.: Ozone sonde cell current measurements and implications for observations of near-zero ozone concentrations in the tropical upper troposphere, Atmos. Meas. Tech., 3, 495–505, doi:10.5194/amt-3-495-2010, 2010. 22174
Walter, R.: CLaMS-Simulation des stratosphärischen Ozonabbaus im antarktischen Winter 2003, Technische Universität Bergakademie Freiberg, Diplomarbeit, 2005. 22176
WMO: Scientific assessment of ozone depletion: 2010, Global Ozone Research and Monitoring Project–Report No. 52, Geneva, Switzerland, 2011. 22174

ACPD
11, 22173–22198, 2011

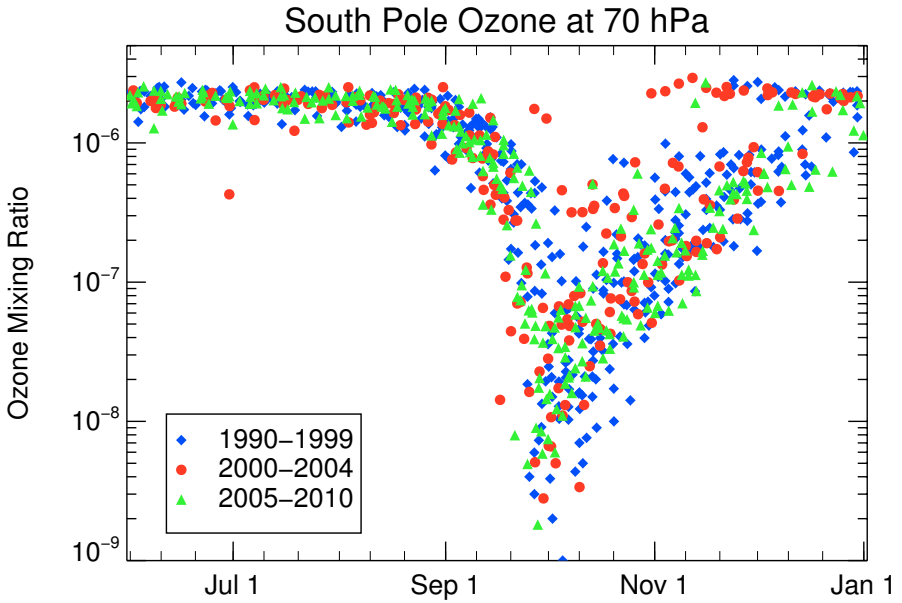

Fig. 1. Ozone observations from South Pole station in winter and spring since 1990. Updated from Fig. 7a of Solomon et al. (2005).

ACPD
11, 22173–22198, 2011

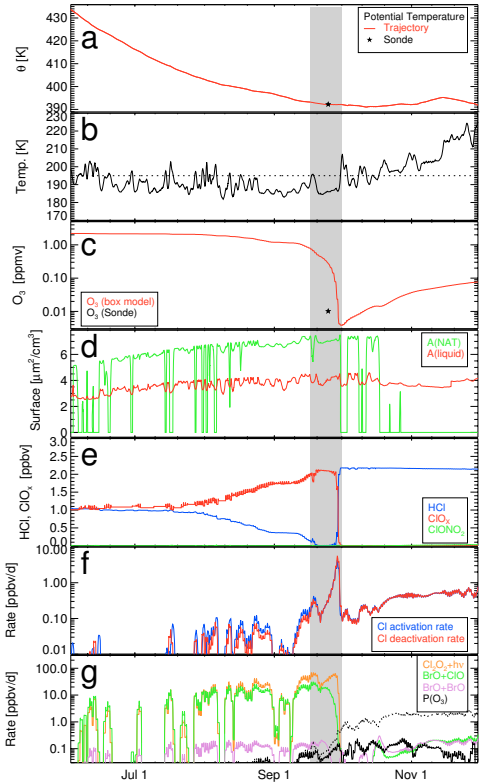

Fig. 2. Trajectory simulations through ozone sonde. The different panels show a time series of the relevant parameters: **(a)** potential temperature of the air parcel, **(b)** temperature, **(c)** ozone (green), minimum vortex ozone (south of 60° S) from 3-D CLaMS (grey), **(d)** Surface area density of NAT and liquid aerosol, **(e)** ClO_x, $ClONO_2$ and HCl, **(f)** net rates of chlorine activation and deactivation, **(g)** rates of catalytic cycles involving ozone. For better clarity, the reaction rates **(f, g)** are plotted as 24 h running average.

ACPD
11, 22173–22198, 2011

Stratospheric ozone chemistry at lowest ozone values

J.-U. Grooß et al.

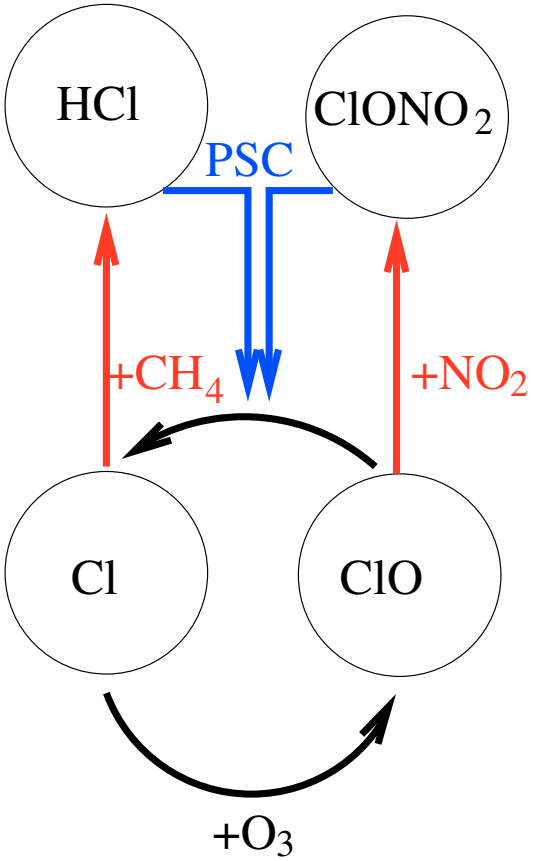

Fig. 3. Sketch of the chlorine activation and deactivation reactions.

ACPD
11, 22173–22198, 2011

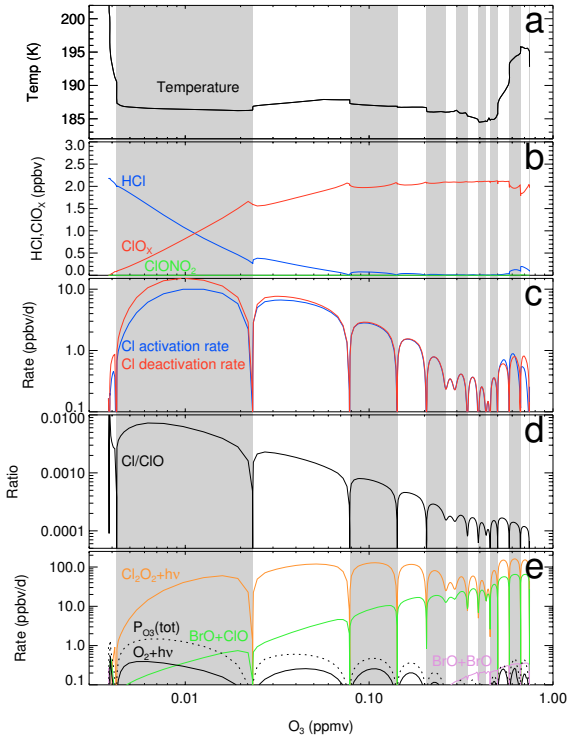

Fig. 4. Parameters before the ozone minimum for the time 17 September–1 October 2003 (grey shaded area in Fig. 2) plotted as function of O_3 mixing ratio. **(a)** temperature, **(b)** chlorine compounds, **(c)** net rates of chlorine activation and deactivation, **(d)** the ratio Cl/ClO, **(e)** rates of catalytic cycles involving ozone. Here, the reaction rates are not plotted as running averages. Thus, the different days of the chosen periods are visible as during night the reaction rates and the Cl concentration typically decrease by many orders of magnitude as Cl_2 is not photolysed during nighttime. The grey shadings correspond to every second day defined by the local maxima of the solar zenith angle.

ACPD
11, 22173–22198, 2011

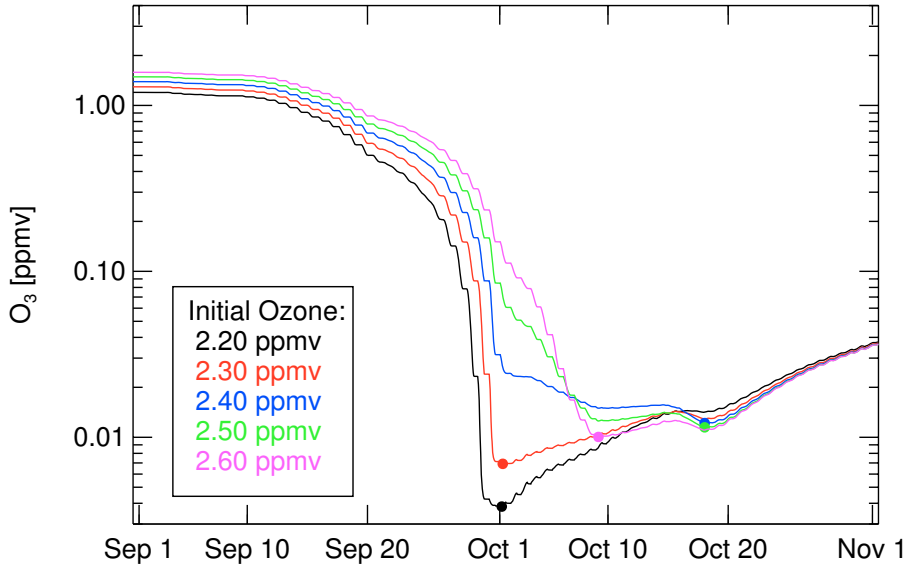

Fig. 5. Sensitivity to ozone initialisation; four additional box model simulations identical to the reference simulation, but with only different initial ozone mixing ratio (see legend). The time of the minimum ozone mixing ratio is marked with a coloured circle.

ACPD
11, 22173–22198, 2011

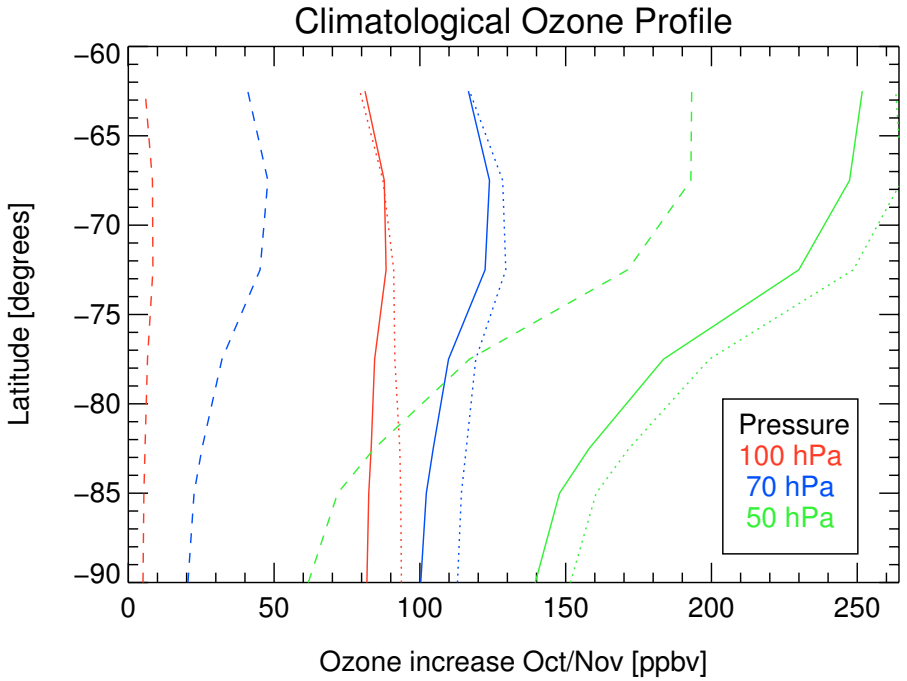

Fig. 6. Simulated ozone increase between 1 October and 30 November as function of latitude for three pressure levels. Solid lines indicate the simulated ozone increase, dashed lines show the ozone increase due to oxygen photolysis (reaction chain 1). Dotted lines show the sum of ozone production by reaction chains 1 to 4.

ACPD
11, 22173–22198, 2011

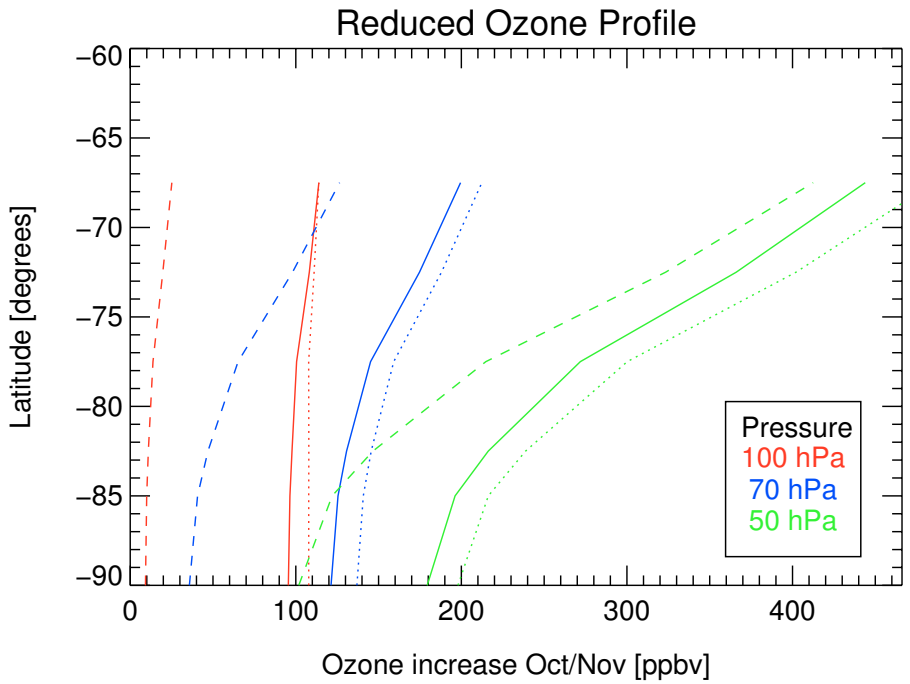

Fig. 7. As Fig. 6, but using a reduced overhead ozone profile (see text).

ACPD
11, 22173–22198, 2011

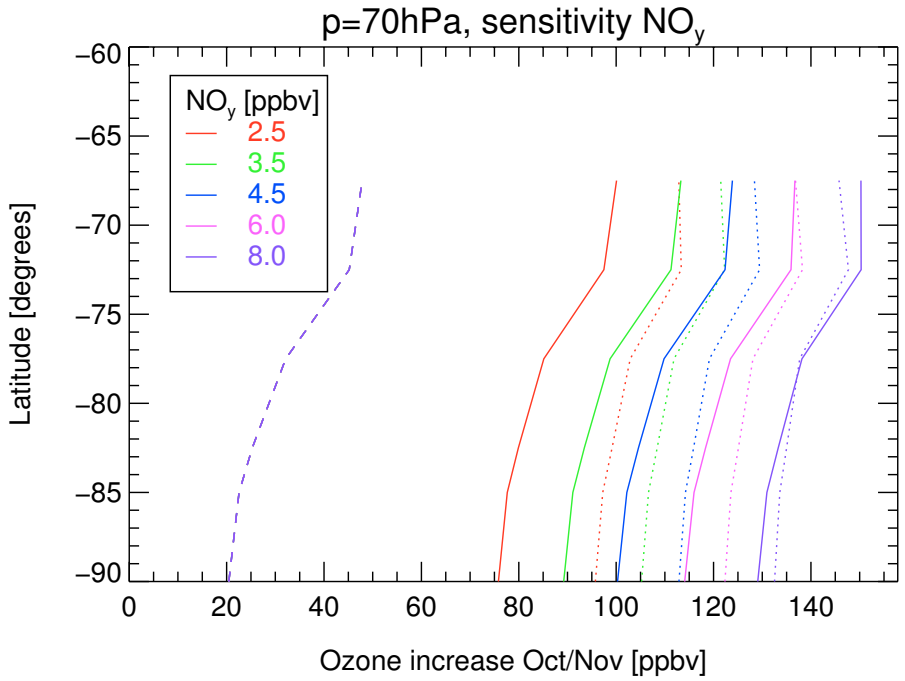

Fig. 8. Simulated ozone increase between 1 October and 30 November for the 70 hPa level (blue line in Fig. 6) for different values of NO_y. The ozone increase due to oxygen photolysis (dashed line) is equal for all simulations.

ACPD
11, 22173–22198, 2011

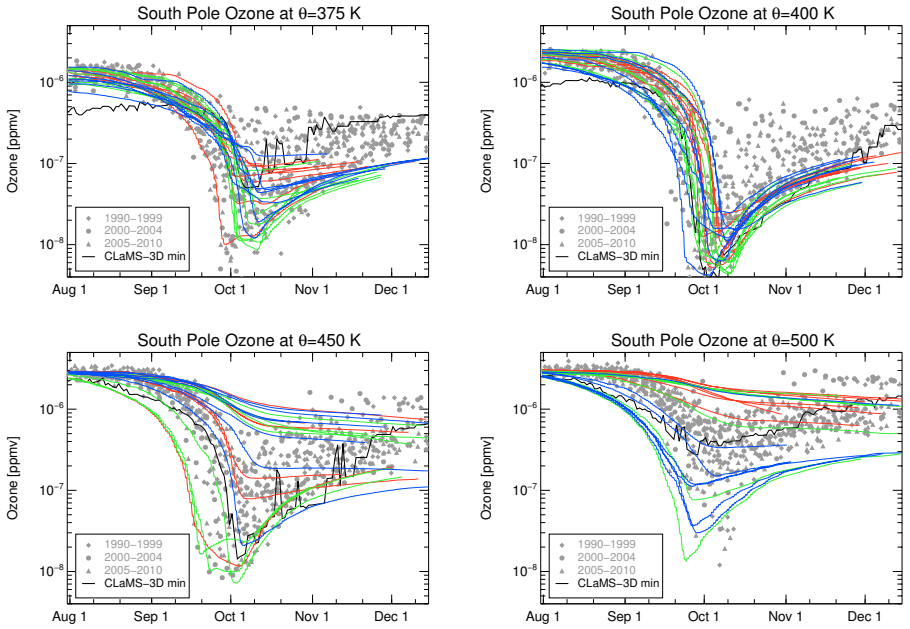

Fig. 9. Comparison of South Pole ozone observations with box model simulations for 4 different levels. The vertical coordinate is potential temperature. South Pole observations for different yeas are plotted as grey symbols. CLaMS box model simulations are shown for 21 trajectories per level that pass the South pole on this level at different times in 2003 (red: 20–26 September; green: 27 September–3 October; blue: 4–10 October). For trajectories that reach latitudes north of 50° S, only the results up to this latitude are shown. The black line corresponds to the minimum ozone mixing ratio of the CLaMS-3D simulation poleward of 75° S for the individual levels.

ACPD
11, 22173–22198, 2011